

Article

Symmetry-Breaking Effect on the Electromagnetic Properties of Plasmonic Trimers Composed of Graphene Nanodisks

Weibin Qiu ^{1,*} , Houbo Chen ¹, Junbo Ren ¹ , Pingping Qiu ¹, Zhili Lin ¹, Jiaxian Wang ¹, Qiang Kan ^{2,3} and Jiaoqing Pan ^{2,3} 

¹ Fujian Provincial Key Laboratory of Light Propagation and Transformation, College of Information Science and Engineering, Huaqiao University, Xiamen 361021, China; 1400201017@hqu.edu.cn (H.C.); 1611301026@hqu.edu.cn (J.R.); 1511301022@hqu.edu.cn (P.Q.); zllin@hqu.edu.cn (Z.L.); wangjx@hqu.edu.cn (J.W.)

² College of Materials Science and Opto-Electronic Technology, University of Chinese Academy of Sciences, Beijing 100083, China; kanqiang@semi.ac.cn (Q.K.); jqpan@semi.ac.cn (J.P.)

³ Key Laboratory of Semiconductor Materials Science, Institute of Semiconductors, Chinese Academy of Science, Beijing 100083, China

* Correspondence: wbqiu@hqu.edu.cn; Tel.: +86-592-6162380

Received: 26 January 2018; Accepted: 28 February 2018; Published: 5 March 2018

Abstract: Plasmonic trimers composed of equal-sized graphene nanodisks are proposed in this paper. The symmetry-breaking effect on the electromagnetic properties of the nanostructure is numerically investigated by studying plasmon energy diagrams and optical scattering spectra in mid-infrared range with a gradient vertex angle. The degenerate plasmonic modes are lifted and new modes appear with increased vertex angle. The energy diagrams are consistent with scattering extinction spectra, about which the dipole moment distribution of the proposed structure is discussed to demonstrate the coupling strength of the collective plasmonic modes of the trimer. More specifically, the frequency tunability of the plasmonic trimer is pointed out by modifying the chemical potential of the graphene nanodisks without varying the geometric configuration. The proposed structure might find applications such as light-matter interaction, single molecule detection, and high-sensitivity chemical sensing.

Keywords: nanomaterials; graphene; trimer; plasmonic molecules; symmetry breaking

1. Introduction

Photonic molecules (PhMs), which are composed of two or more coupled optical microcavities, such as whispering-gallery mode microcavities, Fabry-Perot microcavities, and point-defect microcavities in photonic crystal, have attracted broad attention and undergone intensive investigation since they were introduced [1–3]. An updated version of PhMs, plasmonic molecules (PMs) are metallic nanostructures where the individual plasmon modes interact strongly and show distinct collective behavior [4,5]. Analogous to the phenomena observed in atomic and molecular systems, such as Fano resonances [6–8], slow light [9], and electromagnetically induced transparency [10], interactions between the plasmon modes and the external perturbations also lead to the above-mentioned phenomena in PM systems. Over the past decades, PMs have attracted wide interest for various applications, such as in molecular biology and biomedicine [11]. Recently, Gilad Haran et al. used the multiple multipole program to analyze homologous series of single, dimer, and trimer silver spherical nanoparticle PMs [4,12,13] and showed the changes in plasmonic spectra resulting from modification of the structures with the help of group theory. R. Verre et al. explored the possibility of

broadening the in-plane magnetic response of the metal-insulator-metal dimer [14]. Federico Capasso et al. reported that the optical properties of self-assembled clusters of spherical metal-dielectric colloids were controlled by varying the number and position of particles in the cluster [15]. However, even the best conventional plasmonic materials, such as gold and silver, suffered huge ohmic losses in the frequency regime of interest. Also, once the geometry of PMs is determined, the electromagnetic (EM) properties are unable to tune, which becomes a bottleneck to further progress for metal-based PMs [16].

Recently, graphene, which is composed of a monolayer of carbon, has been widely studied due to its unique advantages in electronics and photonics [17–27]. More specifically, a graphene layer is analogous to a metal sheet that is capable of supporting surface plasmon polariton (SPP) waves [28–30]. Compared with their counterparts supported by conventional plasmonic metals, graphene-supported plasmons demonstrate relatively low damping loss and high confinement [31]. The properties of the plasmon are modified by its surface conductivity, which is further controlled by the chemical potential (Fermi energy) of graphene [32–36]. Nevertheless, the chemical potential is adjustable by means of chemical doping or local gate voltage [37]. Thus, the EM properties of PMs would be more diverse and colorful once the conventional metallic materials are replaced by graphene. We have proposed and investigated the EM properties of plasmonic dimers composed of two graphene nanodisks, including wavelength splitting and coupling, i.e., hybridization of the fundamental and higher-order plasmonic modes [38,39].

To take full advantage of graphene, and to follow the works of Chuntunov and Haran [4,12,13] and exploit their idea, we propose a plasmonic trimer composed of three graphene nanodisks arranged in a triangle, which is much more compact than those composed of conventional metals such as Au and Ag. The properties of plasmonic mode evolution of the nanostructure are studied with gradient lowering of the symmetry. More specifically, frequency tunability is explored without changing the geometry of the nanostructure, which is impossible with conventional metals. Finally, a possible fabrication method is pointed out. The proposed graphene nanostructure might find applications in areas such as chemical sensing, light-matter interaction, etc.

2. Simulation Method and Models

A typical approach to study the optical response of the plasmonic molecule is a semianalytical multiple multipole program [4,12,13] based on boundary discretization. This method was good for understanding the variation of the electromagnetic field with gradient structure modification, and was valid when $ka \ll 1$. Spectra of nanoparticle clusters are analyzed based on their structural symmetry using symmetry-adapted linear combinations of the individual nanoparticle plasmon modes [4]. In this paper, we get the full vertical three-dimensional electromagnetic field (E, H) of the nanostructures by calculating the Maxwell's equations using the finite element method software COMSOL Multiphysics (V5.2, Radio Frequency module, Stockholm, Sweden). Scattering spectra and energy diagrams of the graphene-based trimeric plasmonic molecules are obtained by employing the frequency domain and the eigenfrequency solvers of the commercial software. Then the evolution of the collective mode of the trimer is investigated with the help of irreducible representations of the relevant point group, which is similar to other studies [4,12]. More significantly, the tunable properties of the plasmonic molecule are demonstrated by modifying the chemical potential of the graphene without changing the geometric parameters.

The geometry of the proposed structure is schematically shown in Figure 1a, where three graphene nanodisks are arranged in a triangle and lie on the SiO_2 substrate. The nanocluster is illuminated by transverse magnetic (TM) polarization light with electric field E along the longitudinal direction. The extinction cross-section σ_{ext} , composed of scattering cross-section σ_{sc} and absorption-cross section σ_{abs} , is expressed as

$$\sigma_{ext} = \sigma_{sc} + \sigma_{abs}, \quad (1)$$

with

$$\sigma_{sc} = \frac{1}{I_0} \iint (\vec{n} \cdot \vec{S}_{sc}) dS, \tag{2}$$

where \vec{n} indicates the normal vector pointing outwards from the plasmonic molecule, and \vec{S}_{sc} and I_0 are the scattered intensity (Poynting vector) and the incident electromagnetic energy intensity, respectively. The integral is taken over the closed surface of trimer,

$$\sigma_{abs} = \frac{1}{I_0} \iiint Q dV, \tag{3}$$

where Q is the power loss density in the graphene molecule and the integral is taken over the volume.

The graphene nanodisk is treated as a thin film with an equivalent thickness of Δ in our study. Thus, it is characterized by an equivalent permittivity of $\epsilon_{g,eq}(\Delta)$ [40,41], which is a function of both Δ and the surface conductivity of graphene given by $\epsilon_{g,eq} = -i\sigma_g\eta_0/(k_0\Delta)$. Here, η_0 ($\approx 377 \Omega$) is the impedance of air, $k_0 = 2\pi/\lambda$ represents the wave number of the free space, and σ_g is the contributions from the interband electron-electron transition σ_{inter} and the intraband electron-photon scattering σ_{intra} . According to the Kubo formula [34,42,43], graphene's surface conductivity is written as $\sigma_{total} = \sigma_{inter} + \sigma_{intra}$,

$$\sigma_{inter} = i \frac{e^2}{4\pi\hbar} \ln \left[\frac{2|\mu_c| - \hbar(\omega - i\tau^{-1})}{2|\mu_c| + \hbar(\omega - i\tau^{-1})} \right], \tag{4}$$

$$\sigma_{intra} = i \frac{e^2 k_B T}{\pi \hbar^2 (\omega + i\tau^{-1})} \left[\frac{\mu_c}{k_B T} + 2 \ln(\exp(-\frac{\mu_c}{k_B T}) + 1) \right], \tag{5}$$

where μ_c is chemical potential, which is tunable by either chemical doping or external gate voltage. τ is the momentum relaxation time of electrons, and it is set to 0.5 ps throughout this paper. Twenty cores of Xeon CPU and 512 Gb memory were employed to run the calculations. It took 47 h to complete each run.

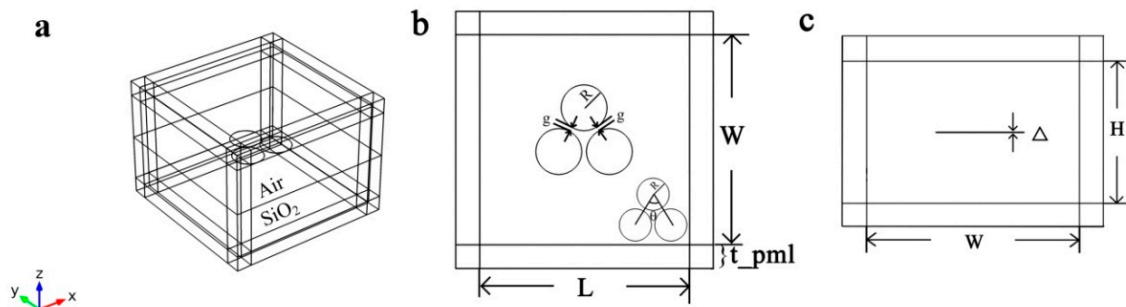


Figure 1. (a) Three-dimensional geometry of the proposed structure: (b) vertical view, (c) left view. Here, the radius (R), height (Δ), and chemical potential (μ_c) of graphene are 50 nm, 0.335 nm, and 0.5 eV, respectively. θ is the vertex angle of trimeric plasmonic molecules (PMs), shown in the inset of (b), and $g = 1$ nm is the distance between the individual plasmonic “atoms.” Outside the graphene is the free space, where the length (L), width (W), and height (H) of the computation window are 450 nm, 450 nm, and 300 nm, respectively.

3. Results and Discussion

3.1. General Depiction of the Mode of Graphene Plasmonic Trimers

The typical induced surface charge density distributions of graphene plasmonic trimers are depicted in the first row of Figure 2. The direction of the dipole of each “atom” is from negative charge to positive charge, and the corresponding dipole distribution of the whole plasmonic molecule is shown in the second row. The A_1' mode in the first column of the first row belongs to the equilateral

triangle (D_{3h} symmetry), which is the highest-symmetry case of a trimeric PM. Here, the direction of the base of the triangle is defined as longitudinal, which in Figure 2 is the x axis. The vertical direction is defined as perpendicular to the base, which in Figure 2 is the y axis. For a succinct expression to describe the distribution of dipole moments, we define the zero net dipole moment along one axis as symmetrical with this axis and the nonzero net dipole moment as asymmetrical. Note that the total moment of the dipole of D_{3h} symmetry is zero due to the symmetry, as shown in the corresponding diagram in the second row of the first column. When the vertex angle of the plasmonic trimer increases, D_{3h} symmetry reduces to C_{2v} symmetry. The total dipole of the whole trimer in the longitudinal direction remains zero, while the counterpart in the vertical direction becomes nonzero, as shown in the second row of Figure 2b. This nonzero momentum suggests that the whole PM is optically active with the polarized light incidents. When the vertex angle becomes 180° , the PM turns out to be a linear chain with a symmetrical group of $D_{\infty h}$, where the electromagnetic field demonstrates a Π_u mode, shown in Figure 2c.

In this paper, only the fundamental mode of each plasmonic atom is considered. So we are only concerned about the point dipole located in the center of each plasmonic atom induced by the surface charge. The properties of the quadrupole induced by the surface charge are beyond the scope of this paper. Note that the incident angle of the light does not have a significant effect on either the near field or the far field of the plasmonic molecule; only the in-plane mode field distribution and the scattering spectra with respect to the normal incident electromagnetic field are considered here. Furthermore, the electromagnetic properties of the plasmonic molecule system are computed by solving the classic Maxwell's equations and the quantum effects, such as electron tunneling between the plasmonic atoms, are ignored, and even the distance between the nanodisks is in nanometer scale.

The trimer plasmonic molecules have six mode categories [2] due to the D_{3h} symmetry, shown in Figure 3. Similar to the molecule orbit, which is composed of linear combinations of each atom, the collective modes of the trimer are made of linear combinations of each plasmonic mode. These six mode categories are divided into two groups, one corresponding to the higher energy of antibonding modes, and the other corresponding to low-energy bonding modes, which is consistent with the plasmon hybridization calculation [1]. In the antibonding group, there are doubly degenerated modes related to the irreducible representation of E' symmetry. In the highest energy E' state, the dipoles of the nanodisks on the base show symmetric distribution with respect to the longitudinal direction, so the nonzero net dipole appears along this direction. In the other E' case, the vertical dipole disappears in the vertex atom of the trimer and the dipoles of the other base atoms arrange symmetrically with respect to the vertical direction. Consequently, it shows the nonzero net dipole along the longitudinal direction. Additionally, there is another nondegenerate mode related to the irreducible representation of A_2' symmetry located at the lower energy state. Interestingly, in this case, the dipole of the vertex atom disappears, similar to the first case of the bonding E' mode. However, the net dipole of the whole trimer system in antibonding A_2' mode is along the longitudinal direction and in the bonding E' mode is along the vertical direction. As for the doubly degenerate bonding E' mode with lower energy, it shows the net dipole along the longitudinal direction. Moreover, among the lower energy state bonding modes, the nondegenerate A_1' is also located at the lowest position, and the dipole of the total plasmonic trimer is centered symmetrically. As a result, the total dipole of the whole plasmonic trimer is zero. As the vertex angle θ increases gradually, the D_{3h} symmetry reduces to lower symmetry C_{2v} , and the plasmonic modes interact with each other, which finally results in lifting the degeneracy of the higher symmetric modes, and new energy states appear, shown in the center columns of Figure 3. The structures of the new plasmonic modes A_1 and B_2 are gradually changed from those of the D_{3h} modes as the vertex angle θ increases. However, the direction of the dipole moment of the vertex nanodisk does not change when the vertex angle increases, while the counterparts in the other two nanodisks on the base rotate synchronously counterclockwise and clockwise. It is noticeable that for the B_2 modes, the nonzero net dipole moment is along the longitudinal direction, while for the A_1 mode, the nonzero net dipole moment is along the vertical direction.

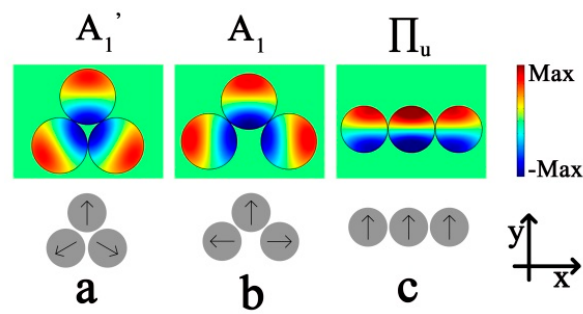


Figure 2. Surface charge density distributions of typical trimeric graphene plasmonic trimers.

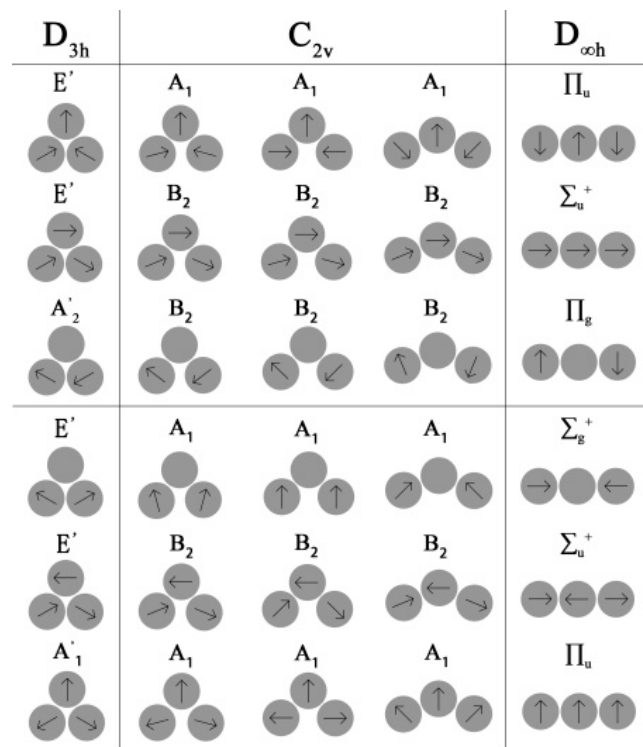


Figure 3. Dipole distributions of graphene plasmonic trimers: equilateral triangle (D_{3h} symmetry) modes (left column), isosceles triangle (C_{2v} symmetry) modes (center columns), and linear chain ($D_{\infty h}$ symmetry) modes (right column).

When the vertex angle further increases to π , the graphene nanodisks become a chain and the trimer molecule shows $D_{\infty h}$ symmetry. The dipole distribution of this symmetry group is illustrated in the right column of Figure 3. The antibonding $E'-A_1$ path evolves to the Π_u mode, where the dipole moment of the center nanodisk is shown upwards and those of the nanodisks on both the sides show reversed vertical direction. The antibonding $E'-B_2$ path evolves to Σ_u^+ mode, and the net dipole moment is three times of that of the center nanodisk, since all the directions of the three nanodisks are identical along the longitudinal direction. The mode of the antibonding $A_2'-B_2$ path becomes Π_g , where the dipole moment of the vertex disks stays at zero and the total is zero. The mode of the bonding $E'-A_1$ path becomes Σ_g^+ . The total dipole moment of this mode is also zero, because the dipole of the center nanodisk disappears, and those of the nanodisks on the two sides are along the reversed longitudinal direction. The bonding $E'-B_2$ path transforms into Σ_u^+ mode and the mode evolution of bonding Σ_u^+ irreducible representation of the $D_{\infty h}$ symmetry group, where the dipole of the center nanodisk points left, while the other two nanodisks in the two sides point right. The mode

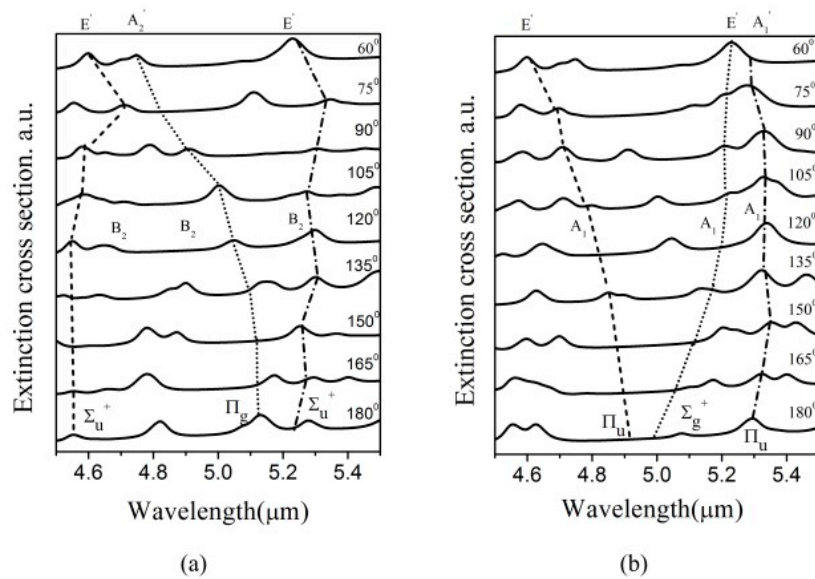


Figure 6. Scattering extinction cross-section as a function of wavelength ranging from 4.5 to 5.5 μm . (a) The incident light is longitudinally polarized, (b) the incident light is vertically polarized.

3.5. Frequency Tunability of Graphene Plasmonic Trimers

To demonstrate the tunable advantage of graphene, we keep the identical geometry of the graphene trimer and change the chemical potential to 0.6 eV. The calculated resonance energy diagram and the corresponding scattering spectra are plotted in Figures 7 and 8. It is seen that the general trend is that the energy diagram and the scattering spectra are identical with those of graphene trimer with a chemical potential of 0.5 eV. The difference is the blue-shift effect in the corresponding spectra and the energy diagrams. This comes from the higher frequency of the eigenmodes of the trimer with a higher chemical potential. Also, the corresponding quality factors are higher due to the lower absorption loss. This property enables the graphene trimer to be flexibly used in a wide spectral range by changing the chemical potential of graphene. This structure will benefit development of multiband graphene nanosensors. It should be noted that the refractive index of the SiO_2 affects the positions of the plasmonic peaks of the scattering spectra. However, it does not influence the mechanism of mode evolution and frequency tunability.

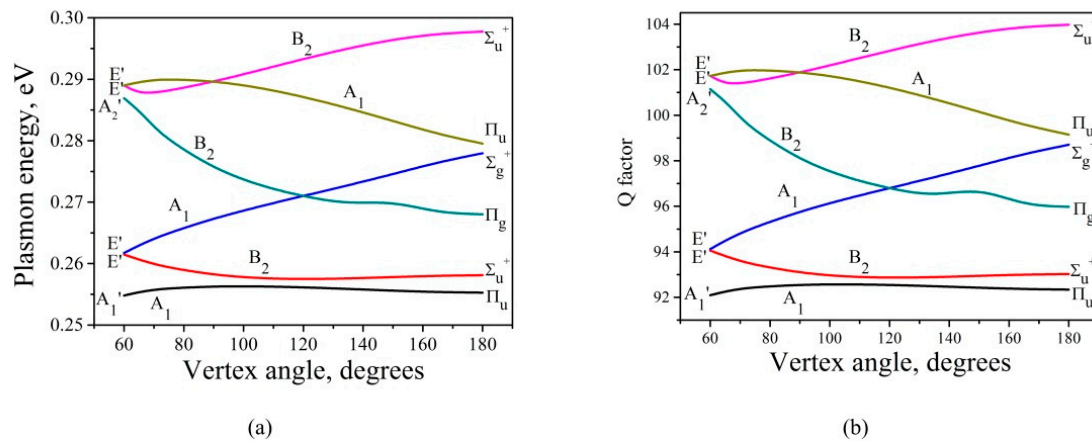


Figure 7. (a) Plasmonic energy diagram of graphene plasmonic trimers. (b) Corresponding quality factors of the plasmon modes as a function of vertex angle. The chemical potential of graphene is 0.6 eV. Compared with trimers of 0.5 eV graphene, the energy diagram shows blue shift, and the corresponding Q factors increase.

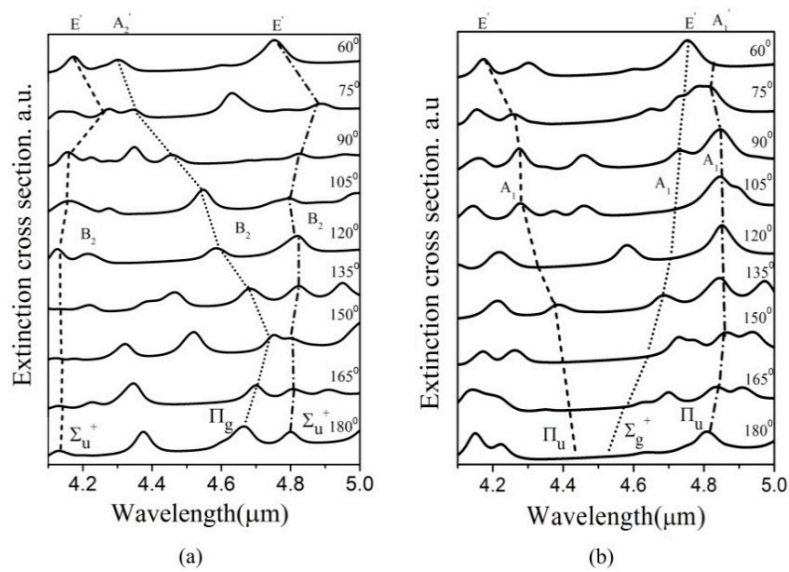


Figure 8. Extinction cross-section spectra of graphene trimers with 0.6 eV chemical potential under linearly polarized mid-infrared light. (a) B_2 modes that are optically active with longitudinal polarization, (b) A_1 modes that are optically active with vertical polarization. Compared with those of 0.5 eV graphene, the corresponding peaks in the spectra show blue shift.

3.6. Fabrication Process Suggestion

In terms of the fabrication process of graphene plasmonic trimers, the graphene monolayer with certain chemical potential, i.e., doping concentration, could be transferred to the SiO_2 substrate. It could also be deposited on the SiO_2 substrate by the chemical vapor deposition technique. Then negative tone electron beam resist is spin-coated on the graphene, followed by the exposure process. Later, the designed patterns are transferred to negative tone electron beam resist after development. As for the periodic patterns, the distance between the neighboring trimers should be far enough to avoid mode coupling between the trimers. Then the patterns are transferred to the graphene monolayer by the reactive ion etching technique, using the electron beam resist as the etching mask. Finally, the remaining resist is totally removed by rinsing the wafer with solvent, and the samples are ready for testing.

4. Summary

In this work, following the works of Chuntunov and Haran [4,12,13] and exploiting their ideas, we propose plasmonic trimer composed of graphene nanodisk with a more compact footprint than the conventional metals. The effect of symmetry of the graphene cluster's electromagnetic properties is numerically investigated by gradually increasing the vertex angle. With increased vertex angle, the symmetry of the plasmonic molecule breaks, and the degenerate plasmonic mode lifts. Consequently, the clusters demonstrate nonzero net dipole moments, which further show optical sensitivity to the specific linear polarization light in the mid-infrared region. The calculated vertex angle-dependent extinction cross-section spectra agree well with the plasmonic energy diagrams. Furthermore, the frequency tunability of the graphene nanostructure is examined by varying the chemical potential without changing the geometry of the proposed structures, which is impossible with the conventional metals. Blue shift of the plasmonic resonant modes is observed with a high chemical potential. The proposed graphene plasmonic trimers could play a significant role in enhancing the performance of optical components based on single whispering-gallery mode nanocavity, such as directional emission nanocavity lasers and high-sensitivity sensors.

Acknowledgments: The authors are grateful for support from the Natural Science Fund of China under grant nos. 11774103, 61378058, and 61575070, Fujian Province Science Funds for Distinguished Young Scholar (no. 2015J06015), and the Promotion Program for Young and Middle-Aged Teachers in Science and Technology Research of Huaqiao University (no. ZQN-YX203).

Author Contributions: Weibin Qiu provided the original idea of this project; Houbo Chen, Pingping Qiu, and Junbo Ren did the simulations; Weibin Qiu, Houbo Chen, Pingping Qiu, Zhili Lin, Junbo Ren, Jiaxian Wang, Qiang Kan, and Jiaoqing Pan analyzed the data; Weibin Qiu, Junbo Ren, and Houbo Chen wrote the paper.

Conflicts of Interest: The authors claim no conflicts of interest regarding this work.

References

1. Ku, J.F.; Chen, Q.D.; Ma, X.W.; Yang, Y.D.; Huang, Y.Z.; Xu, H.L.; Sun, H.B. Photonic-molecule single-mode laser. *IEEE Photonics Technol. Lett.* **2015**, *27*, 1157–1160. [[CrossRef](#)]
2. Kudryashov, A.V.; Boriskina, S.V.; Paxton, A.H.; Benson, T.M.; Sewell, P.; Ilchenko, V.S. Photonic molecules made of matched and mismatched microcavities: New functionalities of microlasers and optoelectronic components. *Proc. SPIE* **2007**, *6452*, 64520X. [[CrossRef](#)]
3. Vahala, K.J. Optical microcavities. *Nature* **2003**, *424*, 839–846. [[CrossRef](#)] [[PubMed](#)]
4. Chuntunov, L.; Haran, G. Trimeric plasmonic molecules: The role of symmetry. *Nano Lett.* **2011**, *11*, 2440–2445. [[CrossRef](#)] [[PubMed](#)]
5. Wang, H.; Brandl, D.W.; Nordlander, P.; Halas, N.J. Plasmonic nanostructures artificial molecules. *Acc. Chem. Res.* **2007**, *40*, 53–62. [[CrossRef](#)] [[PubMed](#)]
6. Mukherjee, S.; Sobhani, H.; Lassiter, J.B.; Bardhan, R.; Nordlander, P.; Halas, N.J. Fano shells: Nanoparticles with built-in fano resonances. *Nano Lett.* **2010**, *10*, 2694–2701. [[CrossRef](#)] [[PubMed](#)]
7. Luk'yanchuk, B.; Zheludev, N.I.; Maier, S.A.; Halas, N.J.; Nordlander, P.; Giessen, H.; Chong, C.T. The Fano resonance in plasmonic nanostructures and metamaterials. *Nat. Mater.* **2010**, *9*, 707–715. [[CrossRef](#)] [[PubMed](#)]
8. Hentschel, M.; Saliba, M.; Vogelgesang, R.; Giessen, H.; Alivisatos, A.P.; Liu, N. Transition from isolated to collective modes in plasmonic oligomers. *Nano Lett.* **2010**, *10*, 2721–2726. [[CrossRef](#)] [[PubMed](#)]
9. Papasimakis, N.; Fedotov, V.A.; Zheludev, N.I.; Prosvirnin, S.L. Metamaterial analog of electromagnetically induced transparency. *Phys. Rev. Lett.* **2008**, *101*, 253903. [[CrossRef](#)] [[PubMed](#)]
10. Liu, N.; Langguth, L.; Weiss, T.; Kastel, J.; Fleischhauer, M.; Pfau, T.; Giessen, H. Plasmonic analogue of electromagnetically induced transparency at the drude damping limit. *Nat. Mater.* **2009**, *8*, 758–762. [[CrossRef](#)] [[PubMed](#)]
11. Willets, K.A.; Van Duyne, R.P. Localized surface plasmon resonance spectroscopy and sensing. *Annu. Rev. Phys. Chem.* **2007**, *58*, 267–297. [[CrossRef](#)] [[PubMed](#)]
12. Chuntunov, L.; Haran, G. Optical activity in single-molecule surface-enhanced raman scattering: Role of symmetry. *MRS Bull.* **2013**, *38*, 642–647. [[CrossRef](#)]
13. Chuntunov, L.; Haran, G. Effect of symmetry breaking on the mode structure of trimeric plasmonic molecules. *J. Phys. Chem. C* **2011**, *115*, 19488–19495. [[CrossRef](#)]
14. Verre, R.; Yang, Z.J.; Shegai, T.; Kall, M. Optical magnetism and plasmonic Fano resonances in metal-insulator-metal oligomers. *Nano Lett.* **2015**, *15*, 1952–1958. [[CrossRef](#)] [[PubMed](#)]
15. Fan, J.A.; Wu, C.; Bao, K.; Bao, J.; Bardhan, R.; Halas, N.J.; Manoharan, V.N.; Nordlander, P.; Shvets, G.; Capasso, F. Self-assembled plasmonic nanoparticle clusters. *Science* **2010**, *328*, 1135–1138. [[CrossRef](#)] [[PubMed](#)]
16. Zhao, J.; Qiu, W.; Huang, Y.; Wang, J.X.; Kan, Q.; Pan, J.Q. Investigation of plasmonic whispering-gallery mode characteristics for graphene monolayer coated dielectric nanodisks. *Opt. Lett.* **2014**, *39*, 5527–5530. [[CrossRef](#)] [[PubMed](#)]
17. Qiu, W.; Liu, X.; Zhao, J.; He, S.; Ma, Y.; Wang, J.-X.; Pan, J. Nanofocusing of mid-infrared electromagnetic waves on graphene monolayer. *Appl. Phys. Lett.* **2014**, *104*, 041109. [[CrossRef](#)]
18. Zhang, H.; Virally, S.; Bao, Q.; Ping, L.; Massar, S.; Godbout, N.; Kockaert, P. Z-scan measurement of the nonlinear refractive. *Opt. Lett.* **2012**, *37*, 1856–1858. [[CrossRef](#)] [[PubMed](#)]
19. Li, Z.Q.; Henriksen, E.A.; Jiang, Z.; Hao, Z.; Martin, M.C.; Kim, P.; Stormer, H.L.; Basov, D.N. Dirac charge dynamics in graphene by infrared spectroscopy. *Nat. Phys.* **2008**, *4*, 532–535. [[CrossRef](#)]

20. Novoselov, K.S.; Geim, A.K.; Morozov, S.V.; Jiang, D.; Katsnelson, M.I.; Grigorieva, I.V.; Dubonos, S.V.; Firsov, A.A. Two-dimensional gas of massless Dirac fermions in graphene. *Nature* **2005**, *438*, 197–200. [[CrossRef](#)] [[PubMed](#)]
21. Ren, J.; Qiu, W.; Chen, H.; Qiu, P.; Lin, Z.; Wang, J.X.; Kan, Q.; Pan, J.Q. Electromagnetic field coupling characteristics in graphene plasmonic oligomers: From isolated to collective modes. *Phys. Chem. Chem. Phys.* **2017**, *19*, 14671–14679. [[CrossRef](#)] [[PubMed](#)]
22. Hwang, E.H.; Das Sarma, S. Dielectric function, screening, and plasmons in two-dimensional graphene. *Phys. Rev. B* **2007**, *75*, 205418. [[CrossRef](#)]
23. Liu, M.; Yin, X.; Ulin-Avila, E.; Geng, B.; Zentgraf, T.; Ju, L.; Wang, F.; Zhang, X. A graphene-based broadband optical modulator. *Nature* **2011**, *474*, 64–67. [[CrossRef](#)] [[PubMed](#)]
24. Mittendorff, M.; Li, S.S.; Murphy, T.E. Graphene-based waveguide-integrated terahertz modulator. *ACS Photonics* **2017**, *4*, 316–321. [[CrossRef](#)]
25. Correas-Serrano, D.; Gomez-Diaz, J.S.; Alu, A.; Melcon, A.A. Electrically and magnetically biased graphene-based cylindrical waveguides: Analysis and applications as reconfigurable antennas. *IEEE Trans. Terahertz Sci. Technol.* **2015**, *5*, 951–960. [[CrossRef](#)]
26. Sensale-Rodriguez, B.; Yan, R.; Zhu, M.; Jena, D.; Liu, L.; Grace Xing, H. Efficient terahertz electro-absorption modulation employing graphene plasmonic structures. *Appl. Phys. Lett.* **2012**, *101*, 261115. [[CrossRef](#)]
27. Qiu, P.; Qiu, W.; Lin, Z.; Chen, H.; Tang, Y.; Wang, J.X.; Kan, Q.; Pan, J.Q. Investigation of the band structure of graphene-based plasmonic photonic crystals. *Nanomaterials* **2016**, *6*, 166. [[CrossRef](#)] [[PubMed](#)]
28. Hanson, G.W. Dyadic green's functions and guided surface waves for a surface conductivity model of graphene. *J. Appl. Phys.* **2008**, *103*, 064302. [[CrossRef](#)]
29. Amanatiadis, S.A.; Kantartzis, N.V.; Tsiboukis, T.D. A loss-controllable absorbing boundary condition for surface plasmon polaritons propagating onto graphene. *IEEE Trans. Magn.* **2015**, *51*, 4. [[CrossRef](#)]
30. Papadimopoulos, A.N.; Amanatiadis, S.A.; Kantartzis, N.V.; Rekanos, I.T.; Zygididis, T.T.; Tsiboukis, T.D. A convolutional PML scheme for the efficient modeling of graphene structures through the ADE-FDTD technique. *IEEE Trans. Magn.* **2017**, *53*, 1–4. [[CrossRef](#)]
31. Zhao, J.; Liu, X.; Qiu, W.; Ma, Y.; Huang, Y.; Wang, J.X.; Qiang, K.; Pan, J.Q. Surface-plasmon-polariton whispering-gallery mode analysis of the graphene monolayer coated ingaas nanowire cavity. *Opt. Express* **2014**, *22*, 5754–5761. [[CrossRef](#)] [[PubMed](#)]
32. Chen, J.; Badioli, M.; Alonso-Gonzalez, P.; Thongrattanasiri, S.; Huth, F.; Osmond, J.; Spasenovic, M.; Centeno, A.; Pesquera, A.; Godignon, P.; et al. Optical nano-imaging of gate-tunable graphene plasmons. *Nature* **2012**, *487*, 77–81. [[CrossRef](#)] [[PubMed](#)]
33. Kim, M.W.; Ku, P.C. Lasing in a metal-clad microring resonator. *Appl. Phys. Lett.* **2011**, *98*, 131107. [[CrossRef](#)]
34. Ju, L.; Geng, B.; Horng, J.; Girit, C.; Martin, M.; Hao, Z.; Bechtel, H.A.; Liang, X.; Zettl, A.; Shen, Y.R.; et al. Graphene plasmonics for tunable terahertz metamaterials. *Nat. Nanotechnol.* **2011**, *6*, 630–634. [[CrossRef](#)] [[PubMed](#)]
35. Ren, J.B.; Wang, G.Q.; Qiu, W.B.; Lin, Z.L.; Chen, H.B.; Qiu, P.P.; Wang, J.X.; Kan, Q.; Pan, J.Q. Optimization of the Fano resonance lineshape based on graphene plasmonic hexamer in mid-infrared frequencies. *Nanomaterials* **2017**, *7*, 238. [[CrossRef](#)] [[PubMed](#)]
36. Amanatiadis, S.; Kantartzis, N. Distortion of surface plasmon polariton propagation on graphene due to chemical potential variation. *Appl. Phys. A* **2016**, *122*, 313. [[CrossRef](#)]
37. Low, T.; Avouris, P. Graphene plasmonics for terahertz to mid-infrared applications. *ACS Nano* **2014**, *8*, 1086–1101. [[CrossRef](#)] [[PubMed](#)]
38. Chen, H.B.; Qiu, W.B.; Qiu, P.P.; Ren, J.B.; Lin, Z.L.; Wang, J.X.; Kan, Q.; Pan, J.Q. Mode coupling properties of the plasmonic dimers composed of graphene nanodisks. *Appl. Sci.* **2017**, *7*, 359. [[CrossRef](#)]
39. Qiu, W.; Huang, Y.; Chen, H.; Qiu, P.; Tang, Y.; Wang, J.-X.; Kan, Q.; Pan, J.-Q. Coupling of whispering-gallery modes in the graphene nanodisk plasmonic dimers. *Plasmonics* **2016**, *12*, 39–45. [[CrossRef](#)]
40. Lu, W.B.; Zhu, W.; Xu, H.J.; Ni, Z.H.; Dong, Z.G.; Cui, T.J. Flexible transformation plasmonics using graphene. *Opt. Express* **2013**, *21*, 10475–10482. [[CrossRef](#)] [[PubMed](#)]
41. Vakil, A.; Engheta, N. Transformation optics using graphene. *Science* **2011**, *332*, 1291–1294. [[CrossRef](#)] [[PubMed](#)]
42. Wang, B.; Zhang, X.; Yuan, X.C.; Teng, J.H. Optical coupling of surface plasmons between graphene sheets. *Appl. Phys. Lett.* **2012**, *100*, 4. [[CrossRef](#)]

43. Gusynin, V.P.; Sharapov, S.G.; Carbotte, J.P. Magneto-optical conductivity in graphene. *J. Phys. Condens. Matter* **2007**, *19*, 25. [[CrossRef](#)]
44. Huang, Y.; Qiu, W.; Lin, S.; Zhao, J.; Chen, H.; Wang, J.-X.; Kan, Q.; Pan, J.-Q. Investigation of plasmonic whispering gallery modes of graphene equilateral triangle nanocavities. *Sci. China Inf. Sci.* **2016**, *59*, 042413. [[CrossRef](#)]



© 2018 by the authors. Licensee MDPI, Basel, Switzerland. This article is an open access article distributed under the terms and conditions of the Creative Commons Attribution (CC BY) license (<http://creativecommons.org/licenses/by/4.0/>).